Evaluation of a PET Prototype using LYSO:Ce Monolithic Detector Blocks

R. Cuerdo, I. Sarasola, P. García de Acilu, J. Navarrete, M. Cañadas, J. C. Oller, J. M. Cela, P. Rato Mendes, *Member, IEEE*, L. Romero, and C. Willmott

***Abstract* – We have analyzed the performance of a PET demonstrator formed by two sectors of four monolithic detector blocks placed face-to-face. Both front-end and read-out electronics have been evaluated by means of coincidence measurements using a rotating ^{22}Na source placed at the center of the sectors in order to emulate the behavior of a complete full ring. A continuous training method based on neural network (NN) algorithms has been carried out to determine the entrance points over the surface of the detectors. Reconstructed images from 1 MBq ^{22}Na point source and ^{22}Na Derenzo phantom have been obtained using both filtered back projection (FBP) analytic methods and the OSEM 3D iterative algorithm available in the STIR software package [1]. Preliminary data on image reconstruction from a ^{22}Na point source with ∅ = 0.25 mm show spatial resolutions from 1.7 to 2.1 mm FWHM in the transverse plane. The results confirm the viability of this design for the development of a full-ring brain PET scanner compatible with magnetic resonance imaging for human studies.**

I. Introduction

A positron emission tomography (PET) scanner based on arrays of avalanche photodiodes (APDs) together with monolithic LYSO:Ce scintillator crystals is being developed for human brain studies inside a clinical magnetic resonance imaging (MRI) equipment. This PET scanner will be made up of 52 detector modules, each one with four double-layer detectors and eight application specific integrated circuits (ASICs). Previously to the fabrication of this complex scanner, it is necessary to develop simpler demonstrators in order to test the performance not only of the detectors and ASICs but also of the read-out electronics and coincidence processing.

The first demonstrator consisted of an experimental setup with two monolithic blocks working in coincidence, which were read out by the first version of our ASIC (VATA240) followed by both external coincidence and digitalization modules [2]. Although this preliminary prototype showed good spatial resolutions and good imaging qualities, we detected some image distortions due to non-linearities close to the edge of the crystals which could not be avoided because of the absence of neighbor blocks.

Manuscript received November 22, 2011. This work was supported in part by the Spanish "Plan Nacional de I+D+I 2004-2007" under Contract MEC-DPI2006-03083.

R. Cuerdo, I. Sarasola, P. García de Acilu, J. Navarrete, M. Cañadas, J. C. Oller, J. M. Cela, P. Rato Mendes, L. Romero, and C. Willmott are with CIEMAT (Centro de Investigaciones Energéticas, Medioambientales y Tecnológicas), Avda. Complutense 40, 28040 Madrid, Spain (phone: +34 913466033, e-mail: Roberto.Cuerdo@ciemat.es).

The second demonstrator, presented in this work, has two sectors of four monolithic detector blocks each placed face-to-face. Due to mechanical limitations, we have considered only the outer layer detectors of our original double-detector design, which was previously validated by means of Monte-Carlo simulations [3]. By increasing the field of view (FoV) of our prototype, we overcome the problems of the previous demonstrator and at the same time we can obtain a better evaluation of the imaging capabilities of our final BrainPET scanner. In addition, this new prototype uses a new version of our ASIC (VATA241) [4]–[5] which, among other improvements, has implemented a constant fraction discriminator (CFD) to generate the trigger signal. On the other hand, this system allows to validate the data readout architecture, the coincidence processing implemented in a Virtex 5 field programmable gate array (FPGA), and the continuous training method required for the complete BrainPET scanner to determine the points of entrance over the surface of our monolithic detector blocks by using neural network (NN) algorithms [6]–[7].

In this work, we report on the performance of this PET demonstrator in terms of energy and spatial resolution as well as its imaging capabilities.

II. Experimental Setup

Our PET demonstrator consists of two air-cooled boxes, with four front-end boards each, connected to a read-out board by means of flat cables (see Fig. 1). These boxes are placed face-to-face with a separation of 40 cm, corresponding to the diameter of the ring in our final BrainPET. In the following sections we describe not only front-end and read-out electronics but also the training method and the image acquisition procedures.

A. Front-end electronics

Each front-end board (see Fig. 2) has a VATA241 ASIC which reads out the charge coming from a monolithic detector block. In our demonstrator, the detector block consists of two blocks, each one made up of a 10 mm thick LYSO:Ce crystal with a trapezoidal shape, optically glued to a pair of magnetically compatible Hamamatsu S8550-02 APD matrices, totaling 8 x 8 light-collecting sensors [2]. The surface of the crystal is covered with a diffuse white reflector in order to improve the light collection on the APD sensors and a black paint which protects the detector blocks against any undesirable visible light. For each crystal, the ASIC collects the charge from the 64 APD pixels, and delivers 16 analog

signals which correspond to the sums along the eight rows and eight columns of the APD matrix, as well as a common trigger provided by a CFD. These output signals are sent to the read-out electronics where they are digitalized and processed. Front-end boards are electrically separated from the read-out electronics by means of several HCPL-063L optocouplers which isolate their grounds and both positive (1.5 V) and negative (-2 V) power supplies. Doing so, we reduce the noise and the coupling of spurious signals into the ASIC.

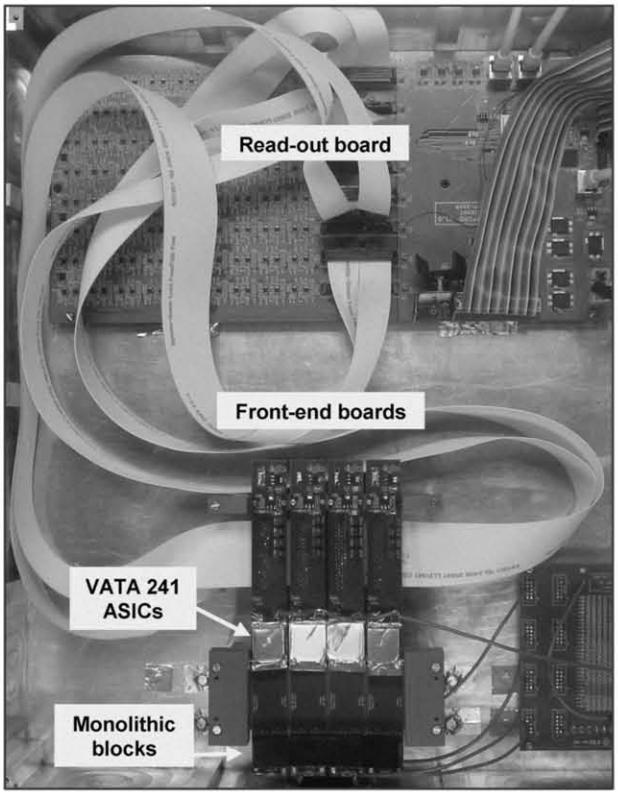

Fig. 1. Photograph of one air-cooled box, showing the read-out and the four front-end boards with the ASICs and the monolithic detector blocks.

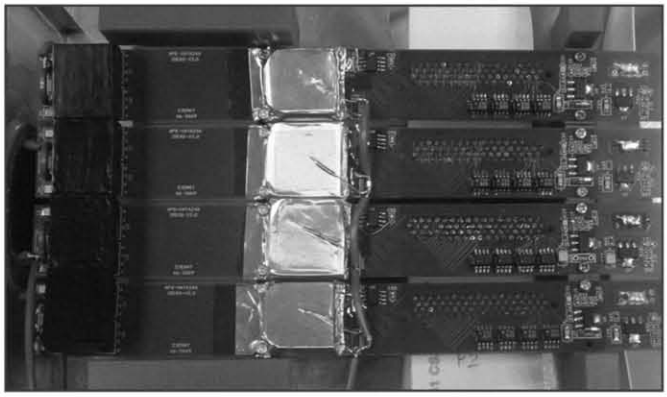

Fig. 2. Photograph of a sector with four front-end boards. The monolithic detector blocks are placed on the left. The ASICs are shielded with a square lid covered in copper foil.

Every APD array requires a specific high voltage bias for a fixed gain. We have biased the APDs 20 V above their nominal voltage in order to obtain gains of about 100, so a separate board with resistance divisors is placed close to the four front-end boards to individually distribute high voltage to each APD sub-array.

B. Read-out electronics

There is a read-out board in each box which captures the data coming from the front-end boards. The 16 differential current output signals provided by every ASIC are sent to the read-out, which convert them to single-ended voltage signals that are digitalized using 12-bit ADCs. The trigger signals are handled by a Virtex 5 FPGA which checks if a coincidence happens within a window of 50 ns, with a time stamp resolution of 2.5 ns. When this occurs, the output data of the ASICs in coincidence is sent to a PC, together with the detector block identifier. After data taking, this information is used for image reconstruction.

C. Training method

Before the image acquisition, it is necessary to estimate the entrance position of coincidence gamma rays over the detector surface. This is carried out thanks to artificial NN algorithms, which after a proper training, allow the calculation of lines-of-response (LoRs) taking into account the projection angle defined by the source holder.

The training is performed by placing a rotating 1 MBq ^{22}Na point source with $\varnothing$ = 0.25 mm close enough to the trained crystal (~21 mm). The rotation is achieved by means of a motorized rotation stage, controlled by a PC, with 0.01° precision placed between the two sectors of monolithic blocks. In addition, there are 3-axis manual position stages to move the source along the FoV in the transverse plane and axial axis with 1 μm precision (see Fig. 3).

This way, 1 mm photon beam widths are obtained over the surface of the monolithic block [8]. These positions over the detector surface are defined by the acceptance angle between this trained crystal, the source, and the other four detectors in coincidence.

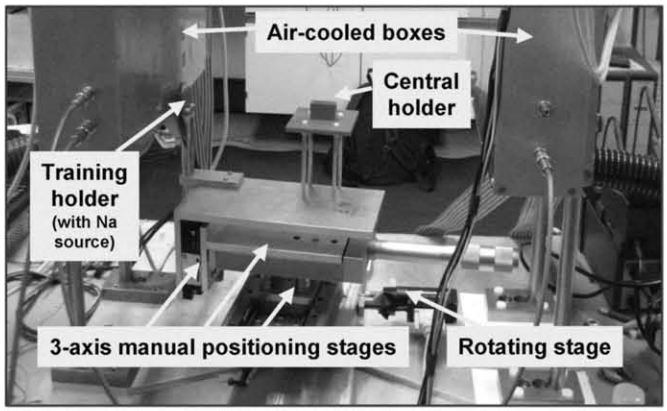

Fig. 3. Photograph of the setup with the two air-cooled boxes, the stages for positioning the source, and the two holders for training and imaging acquisition.

D. *Imaging acquisition*

Once the training is completed, the acquisition of coincidence data at different projection angles for ^{22}Na point source and Derenzo phantom can be performed with the aim of obtaining images.

The sources are placed at the central holder of the prototype, and rotated 360º in steps of 3º. They can also be placed at different positions along the FoV by means of the 3-axis manual position stages. We have acquired around 200,000 coincidence events per single image for the point sources and around 9.6 million coincidence events for the Derenzo source, in order to obtain good enough quality images.

The image reconstruction is carried out by means of the SSRB-FBP-2D (Single Slice Rebinning followed by Filtered Back Projection) analytic algorithm and the OSEM 3D iterative algorithm from the STIR package for tomographic reconstruction [1].

III. Results

The performance of a PET demonstrator with eight monolithic detector blocks has been studied in terms of energy resolution, spatial resolution at detector level after the NN training method, and reconstructed image quality.

A. *Energy resolution*

Fig. 4 shows the energy spectra of a detector block obtained with a single front-end board using ^{22}Na and ^{137}Cs sources. Although the measured energy resolution at 511 keV is 22.0 % FWHM, this represents an upper limit since the APD-input routings of these front-end boards are fabricated in FR4 material instead of flexible Kapton tape (which has less capacitance), and the ASIC noise is strongly dependent on the capacitance at inputs. These results will be improved in the final BrainPET.

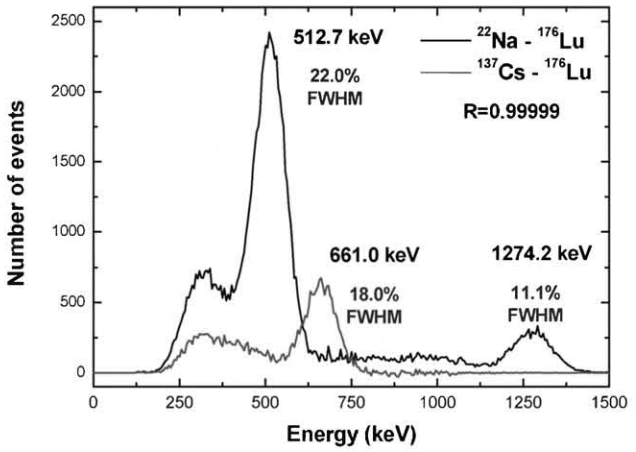

Fig. 4. Energy spectra obtained for a monolithic detector block with an APD overbias of 20 V using ^{22}Na and ^{137}Cs sources, subtracting the ^{176}Lu background from LYSO:Ce crystals.

B. *Spatial resolution from NN algorithms*

Several types of NN algorithms have been tried for our monolithic detector blocks. We have achieved an optimal spatial resolution with a two-step Feed Forward Neural Network (NN^{G+L}) [8].

Table I shows the measured spatial resolutions at detector level obtained after the training procedure. Detectors in each box are labeled as B0, B1, B2 and B3. Resolutions are between 2.1 to 2.4 mm FWHM in the centered blocks (grey lines), whereas in the lateral blocks the spatial resolution worsens to 2.3 to 2.7 mm FWHM.

TABLE I. FWHM SPATIAL RESOLUTION FOR THE COINCIDENCES BETWEEN DETECTOR BOXES 1 AND 2

FWHM (mm) ↓ Box 1 vs Box 2 →	**B0**	**B1**	**B2**	**B3**
B0	2.70	2.33	2.30	2.36
B1	2.33	2.17	2.13	2.27
B2	2.36	2.20	2.20	2.30
B3	2.73	2.50	2.63	2.63

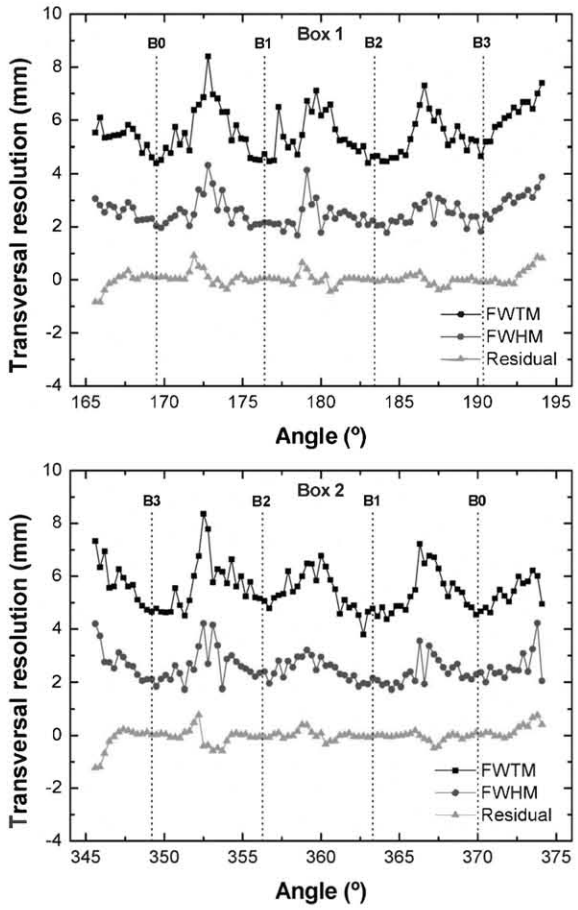

Fig. 5. FWTM and FWHM transversal resolution of the detectors located in box 1 (top) and box 2 (bottom). The residual is also shown, which is the difference between the real value of a specific angle and the output value obtained by the NN for that angle. The four blocks in each box are labeled as B0, B1, B2 and B3. The center of each detector is indicated by a dotted line.

The FWHM and FWTM of the spatial resolutions along the transversal axis of both boxes are shown in Fig. 5. Detector blocks show a good linearity over their surface, which is clearly observed in terms of their flat residual; although there are some non-linearities at their edges due to the absence of neighbor blocks. In addition, gaps up to 1 mm between consecutive blocks also produce some degradation in the spatial resolution.

C. *Image reconstruction*

After completing the training of the NN algorithms, the LoRs obtained from coincidence data for a single ^{22}Na source and a ^{22}Na Derenzo phantom can be calculated. Images from the ^{22}Na point source have been reconstructed using the SSRB-FBP-2D analytic algorithm from 3D data, whereas images from the ^{22}Na Derenzo phantom have been obtained by means of the OSEM 3D iterative algorithm available in STIR.

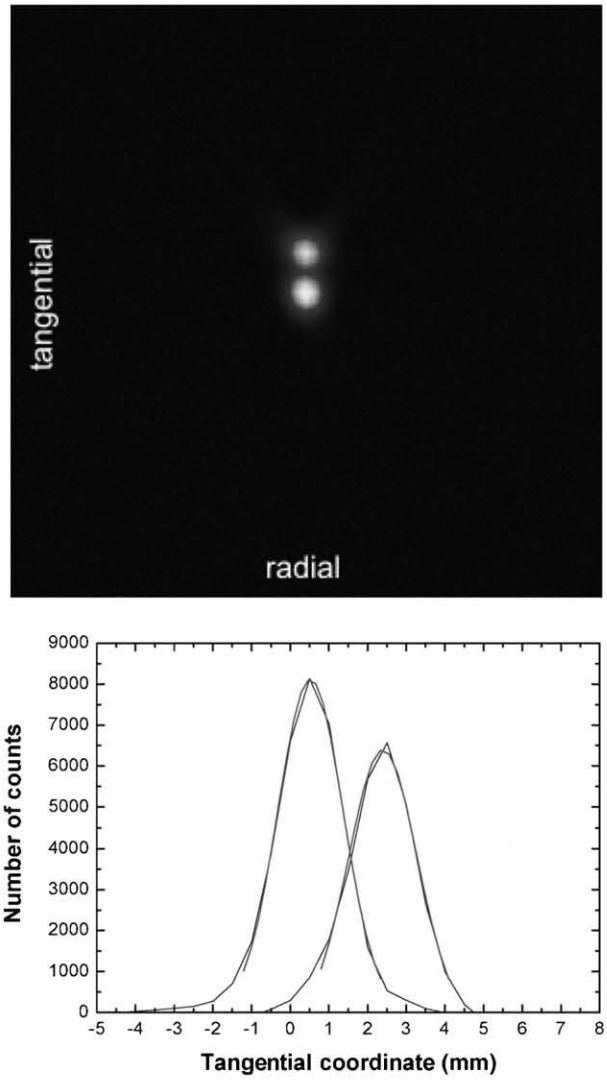

Fig. 6. Transverse image of a single ^{22}Na point source at two different positions separated 2 mm along the tangential direction reconstructed with a pixel size of 0.5 mm (top), and tangential profile for a fixed radial position (bottom).

Fig. 6 shows the superposed image of 1 MBq single ^{22}Na point source with ∅ = 0.25 mm at two different positions separated 2 mm along the tangential direction of the transverse plane, keeping constant the radial coordinate. The reconstruction has been carried out by means of the SSRB-FBP-2D algorithm. Spatial resolutions between 1.7 and 1.9 mm FWHM in the radial direction and between 2.0 and 2.1 mm FWHM in the tangential direction are obtained.

An image of a 1 MBq ^{22}Na Derenzo sealed phantom has also been reconstructed by means of the OSEM 3D iterative reconstruction from the STIR software without any correction or filter applied. The Derenzo phantom has five groups of rods with diameters of 1.2, 1.5, 2.0, 2.5 and 3.0 mm separated a distance two times their diameter (Fig. 7).

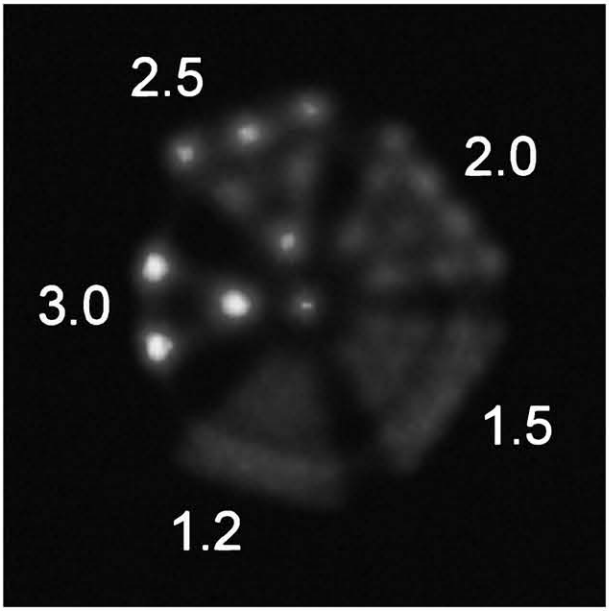

Fig. 7. Image of a ^{22}Na Derenzo sealed phantom reconstructed with a pixel size of 0.5 mm.

IV. Conclusions

The performance of a PET prototype has been validated in terms of the front-end electronics, the data read-out architecture focusing on the coincidence processing, and the new updated ASIC VATA241. The continuous NN training method has been successfully tested, giving spatial resolutions at detector level from 2.1 to 2.4 mm FWHM, similar to the results achieved in our previous demonstrator. Regarding the image reconstruction, preliminary results of ^{22}Na point source and Derenzo phantom have been reported, with reconstructed spatial resolutions at image level from 1.7 to 2.1 mm FWHM in the transverse plane.

Acknowledgment

Authors would like to thank David Francia from CIEMAT for his help in the wire bonding process of the VATA241 ASICs.

REFERENCES

[1] STIR: Software for Tomographic Image Reconstruction [Online]. Available: http://stir.sourceforge.net/

[2] I. Sarasola, P. Rato Mendes, P. García de Acilu, M. Cañadas, O. Vela, J.M. Cela, J.C. Oller, C. Willmott, L. Nuñez, and J.M. Pérez, "PET Demonstrator for a Human Brain Scanner Based on Monolithic Detector Blocks," *IEEE Trans. Nucl. Sci.*, vol. 58, no. 5, pp. 2190-2197, Oct. 2011.

[3] P. Rato Mendes, P. Bruyndonckx, M. Cañadas, Z. Li, J. M. Pérez, and I. Sarasola, "Optimization of a monolithic detector block design for a prototype human brain PET scanner," *2008 IEEE Nucl. Sci. Symp. Conf. Rec.*, pp. 4927-4930, 2008.

[4] I. Sarasola, P. Rato Mendes, R. Cuerdo, P. García de Acilu, J. Navarrete, J. M. Cela, L. Romero, and J. M. Pérez, "A novel front-end chip for a human PET scanner based on monolithic detector blocks," *JINST - Conf. Proc. of the 12th Int. Work. on Rad. Imag. Det.*, vol. 6, C01034, Jan. 2011.

[5] I. Sarasola, R. Cuerdo, J. Navarrete, P. García de Acilu, P. Rato Mendes, L. Romero, and C. Willmott, "Characterization of the VATA 241 front-end ASIC for the BrainPET scanner," *2011 IEEE Nucl. Sci. Symp. Conf. Rec. (MIC15.S-98).*

[6] P. Bruyndonckx, C. Lemaître, D. Schaart, M. Maas, D. J. van der Laan, M. Krieguer, O. Devroede, and S. Tavernier, "Towards a continuous crystal APD-based PET detector design," *Nucl. Instr. Meth. in Phys. Res. A*, vol. 571 pp. 182-186, Feb. 2007.

[7] P. Bruyndonckx, L. Zhi, C. Lemaitre, J. M. Perez, P. Rato Mendes, D. Schaart, M. Maas, D. J. Van der Laan, S Tavernier, and W. Yonggang, "Impact of instrumentation parameters on the performance of neural network based positioning algorithms for monolithic scintillator blocks," *2007 IEEE Nucl. Sci. Symp. Conf. Rec.*, pp. 4266-4270, 2007.

[8] P. García de Acilu, I. Sarasola, M. Cañadas, R. Cuerdo, P. Rato Mendes, L. Romero, and C. Willmott, "Study and optimization of positioning algorithms for monolithic PET detector blocks," *JINST - 9th Int. Conf. on Position Sensitive Detectors PSD9*, Sep. 2011 [in press].